Supporting Information

Nanomechanical Investigations of Crystals of Copper Nanocluster Isomorphs: Enhanced Hardness of the Low-Density Analogue

Amoghavarsha Ramachandra Kini,[a$] Sanghamitra Debta,[b$] Arijit Jana,[a$] C. Aparna,[c] Vivek Yadav,[a] Nataliia Kusiak,[d] Tomas Base,[d] Umesh V. Waghmare,*[e] Pijush Ghosh,*[b] and Thalappil Pradeep*[a]*

[a] *Department of Chemistry, DST Unit of Nanoscience (DST UNS) and Thematic Unit of Excellence (TUE), Indian Institute of Technology Madras, Chennai 600036, India. E-mail: pradeep@iitm.ac.in*

[b] *Department of Applied Mechanics & Biomedical Engg., Indian Institute of Technology Madras, Chennai 600036, India. E-mail: pijush@iitm.ac.in*

[c] *Theoretical Sciences Unit, Jawaharlal Nehru Centre for Advanced Scientific Research, Bengaluru, Karnataka 560064, India. E-mail: waghmare@jncasr.ac.in*

[d] *Department of Synthesis, Institute of Inorganic Chemistry, The Czech Academy of Science 1001, Husinec – Rez, 25068, Czech Republic. E-mail: tbase@iic.acs.cz*

[e] *Theoretical Sciences Unit and School of Advanced Materials (SAMat), Jawaharlal Nehru Centre for Advanced Scientific Research, Bengaluru, Karnataka 560064, India. E-mail: waghmare@jncasr.ac.in*

[$] *These authors contributed equally to this work.*

Table of contents:

Items	Contents	Page No
Table S1	Intercluster interactions present in the crystals of $Cu_4(oCBT)_4$ and $Cu_4(mCBT)_4$ with their distances.	4
Table S2	A comparison of lattice parameters and density obtained from DFT calculations and experiments.	4
Table S3	Estimates of effective and bare Young's moduli of $Cu_4(oCBT)_4$ and $Cu_4(mCBT)_4$, compared with experiments.	5

Figure S1	UV-visible absorption spectra of $Cu_4(oCBT)_4$ and $Cu_4(mCBT)_4$	5
Figure S2	Photoluminescence excitation and emission spectra of $Cu_4(oCBT)_4$ and $Cu_4(mCBT)_4$ crystals	6
Figure S3	XPS spectrum of $Cu_4(oCBT)_4$ nanocluster showing the chemical purity of the sample.	7
Figure S4	XPS spectrum of $Cu_4(mCBT)_4$ nanocluster showing the chemical purity of the sample.	8
Figure S5	Thermogravimetric analysis of $Cu_4(mCBT)_4$ crystals showing the thermal stability of the nanocluster.	9
Figure S6	ATR- IR spectra of heat treated $Cu_4(oCBT)_4$ crystals showing the chemical stability of the samples up to 150°C.	10
Figure S7	ATR- IR spectra of heat treated $Cu_4(mCBT)_4$ crystals showing the chemical stability of the samples up to 150°C.	11
Figure S8	Face indexing of hexagonal $Cu_4(oCBT)_4$ single crystal from two different orientations.	12
Figure S9	Face indexing of hexagonal $Cu_4(mCBT)_4$ single crystal from two different orientations.	12
Figure S10	Arrangement of $Cu_4(oCBT)_4$ clusters in the crystal.	13
Figure S11	Arrangement of $Cu_4(mCBT)_4$ clusters in the crystal.	14
Figure S12	Load-controlled load-displacement curves at a load of 500 µN at different load functions.	15
Figure S13	Load-controlled load-displacement curves at loads of 1000 µN and 5000 µN at different load functions.	15
Figure S14	Displacement-controlled load-displacement curves at displacements of 100 and 500 nm.	16
Figure S15	. Load-displacement curves of all the indentation measurements for $Cu_4(oCBT)_4$ and $Cu_4(mCBT)_4$ at different loads.	16
Figure S16	Statistical analysis of all the indentation data collected for $Cu_4(oCBT)_4$ nanocluster crystal.	17
Figure S17	Statistical analysis of all the indentation data collected for $Cu_4(mCBT)_4$ nanocluster crystal.	17

Figure S18	Load-displacement curves representing indentation induced hardness.	18
Figure S19	SPM images, surface roughness and height profile of $Cu_4(oCBT)_4$ nanocluster crystal surface after nanoindentation.	19
Figure S20	SPM images, surface roughness and height profile of $Cu_4(mCBT)_4$ nanocluster crystal surface after nanoindentation.	20
Figure S21	Arrangement of Cu_4 nanoclusters and CBTs in the ab plane of $Cu_4(oCBT)_4$.	21
Figure S22	Arrangement of Cu_4 nanoclusters and CBTs in the ab plane of $Cu_4(mCBT)_4$.	21

Table S1. Intercluster interactions present in the crystals of $Cu_4(oCBT)_4$ and $Cu_4(mCBT)_4$ with their distances.

$Cu_4(oCBT)_4$		$Cu_4(mCBT)_4$	
Interactions	**Distance**	**Interactions**	**Distance**
S••H-C	2.80 Å	C-H••S	2.81 Å
B-H••H-B	2.32 Å	B-H••S	2.86 Å
B••H-B	3.06 Å	B-H••H-B	2.39 Å
C-H••B(B)	3.04 Å (3.06 Å)	B-H••B	3.10 Å
		B-H••B(B)	2.96 Å (3.14) Å

Table S2. A comparison of lattice parameters and density obtained from DFT calculations and experiments.

Lattice parameters	$Cu_4(oCBT)_4$			$Cu_4(mCBT)_4$		
	DFT value	**Experimental**	**Deviation (%)**	**DFT value**	**Experimental**	**Deviation (%)**
a (Å)	11.23	11.43	-1.75	11.29	11.40	-0.96
b (Å)	11.23	11.43	-1.75	11.61	11.95	-2.85
c (Å)	28.73	29.44	-2.41	31.15	32.31	-3.59
α	90°	90°	0	90°	90°	0
β	90°	90°	0	89.61°	91.20°	-1.74
γ	120°	120°	0	90°	90°	0
Density (g/cm^3)	1.52	1.428	6.44	1.55	1.442	7.49

Table S3. Estimates of effective and bare Young's moduli of $Cu_4(oCBT)_4$ and $Cu_4(mCBT)_4$, compared with experiments.

Parameters	$Cu_4(oCBT)_4$	$Cu_4(mCBT)_4$
E_{bare}	232 GPa	234 GPa
$E_{elastic}$	12.9 GPa	10.1 GPa
$E_{experimental}$	9.79 GPa	8.54 GPa
Density (DFT)	1.52 g/cm^3	1.55 g/cm^3

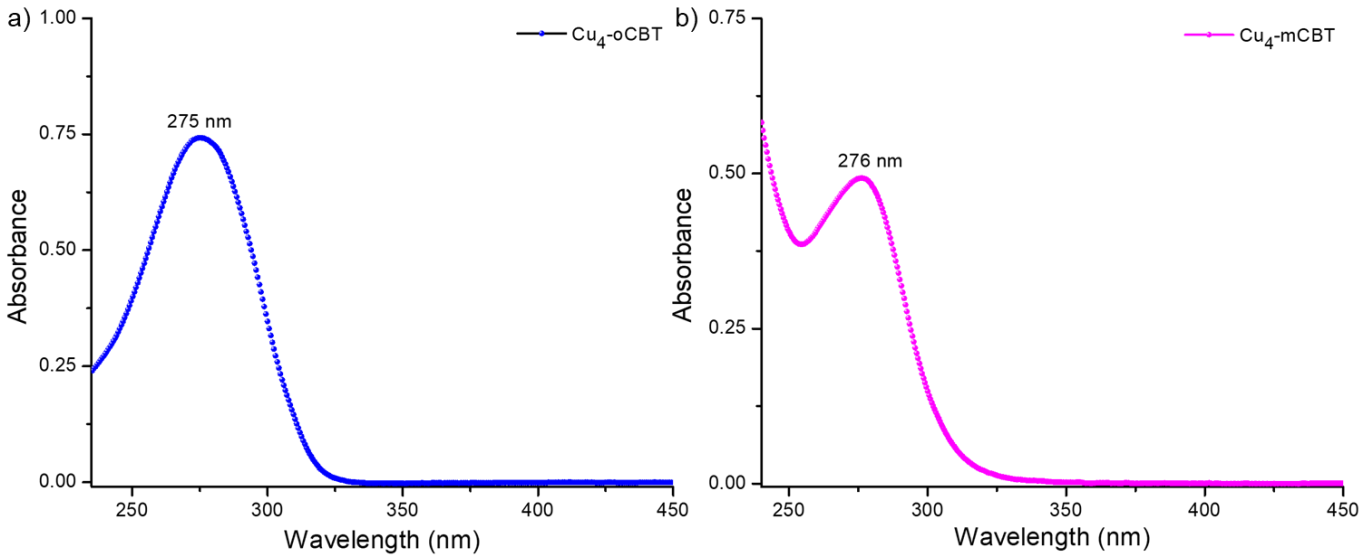

Figure S1. UV-visible absorption spectra of $Cu_4(oCBT)_4$ and $Cu_4(mCBT)_4$ in acetonitrile upon dissolving a few crystals.

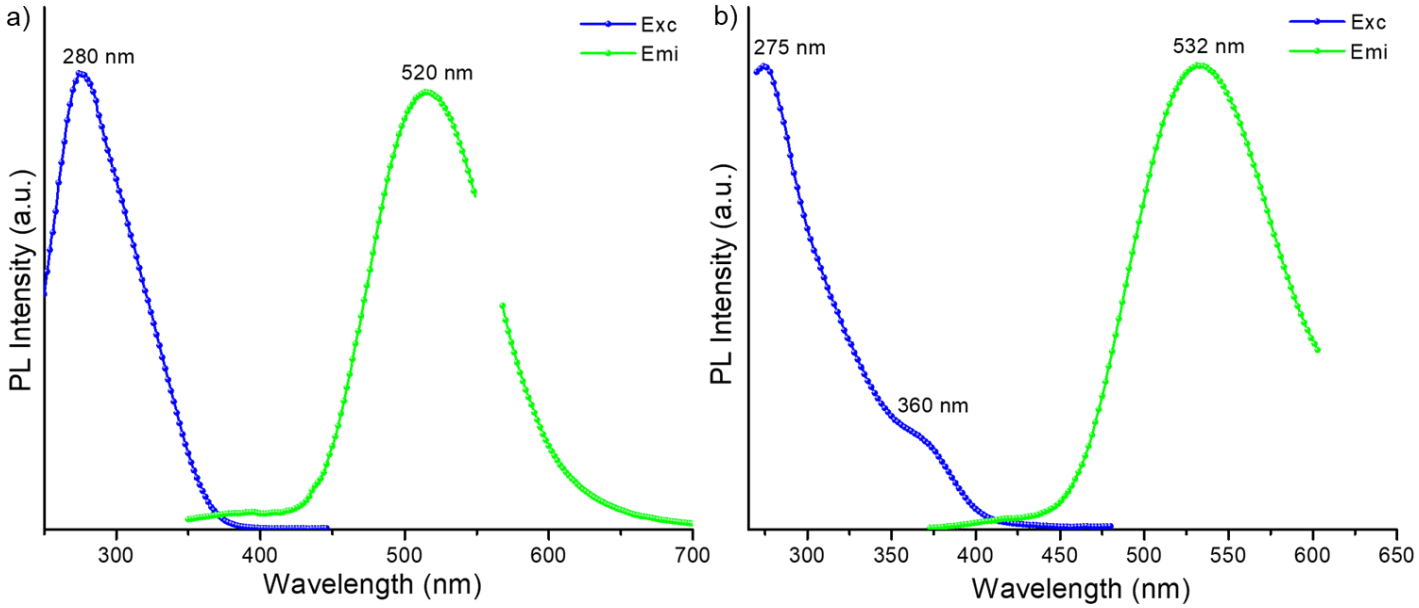

Figure S2. Solid state photoluminescence excitation and emission spectra of $Cu_4(oCBT)_4$ and $Cu_4(mCBT)_4$ crystals.

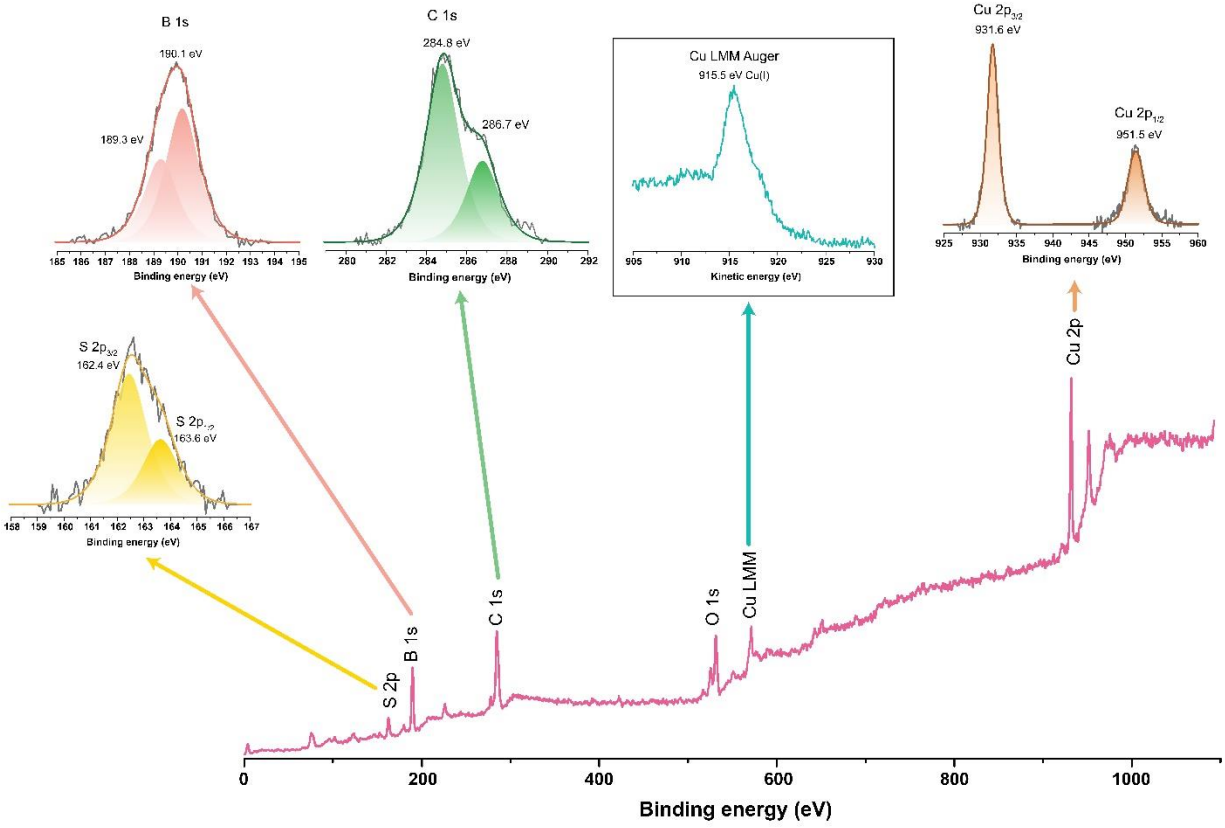

Figure S3. XPS spectra of $Cu_4(oCBT)_4$ crystals. Survey spectra showing the presence of respective elements of the cluster along with detailed spectra of C 1s (green), B 1s (pink), S 2p (yellow) and Cu 2p (orange). The Cu LMM Auger peak is shown within the box. Note that the x-axis is Kinetic Energy.

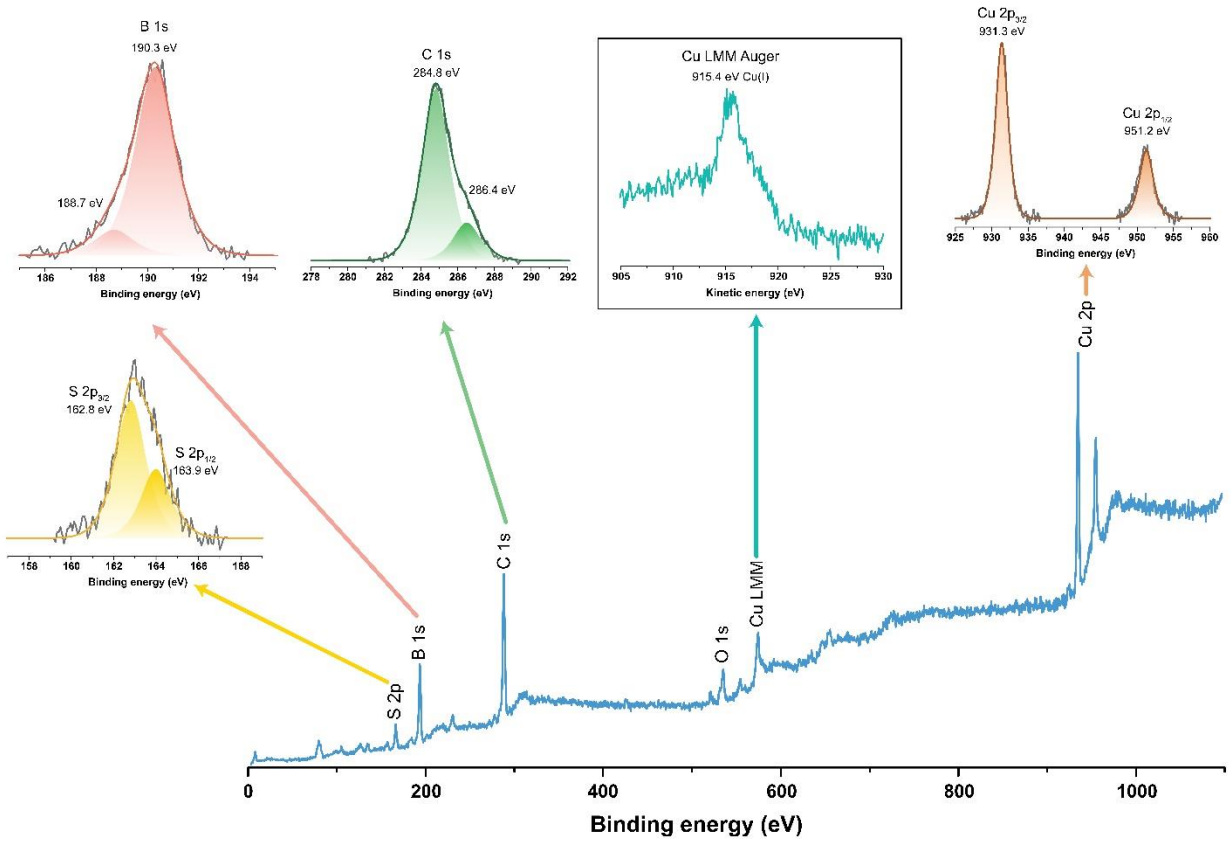

Figure S4. XPS spectra of $Cu_4(mCBT)_4$ crystals. Survey spectra showing the presence of respective elements of the cluster along with detailed spectra of C 1s (green), B 1s (pink), S 2p (yellow) and Cu 2p (orange). The Cu LMM Auger peak is shown within the box. Note that the x-axis is Kinetic Energy.

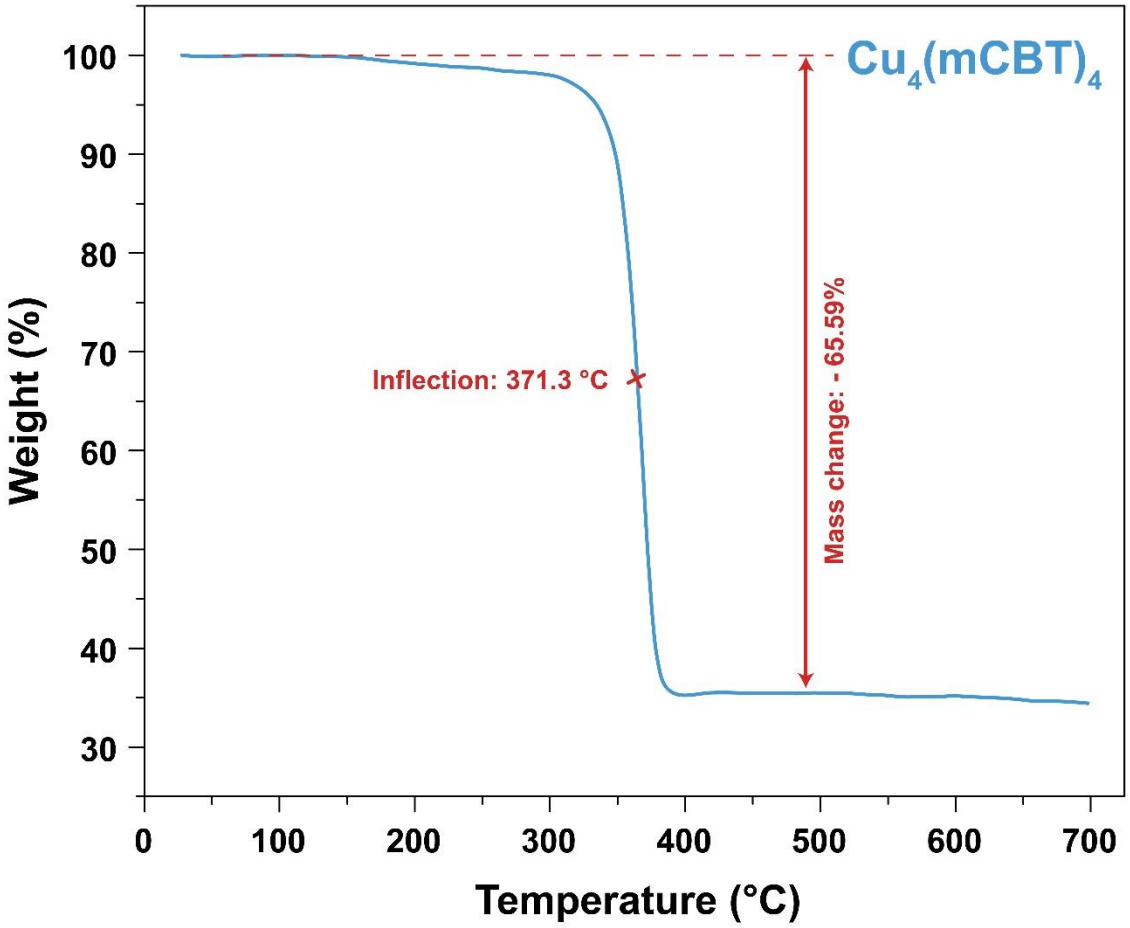

Figure S5. Thermogravimetric analysis of $Cu_4(mCBT)_4$ crystals showing thermal stability up to 370 °C. The cluster $Cu_4(oCBT)_4$ is stable up to 380 °C. Data corresponding to $Cu_4(mCBT)_4$ crystals alone are presented as these have been discussed previously.[1]

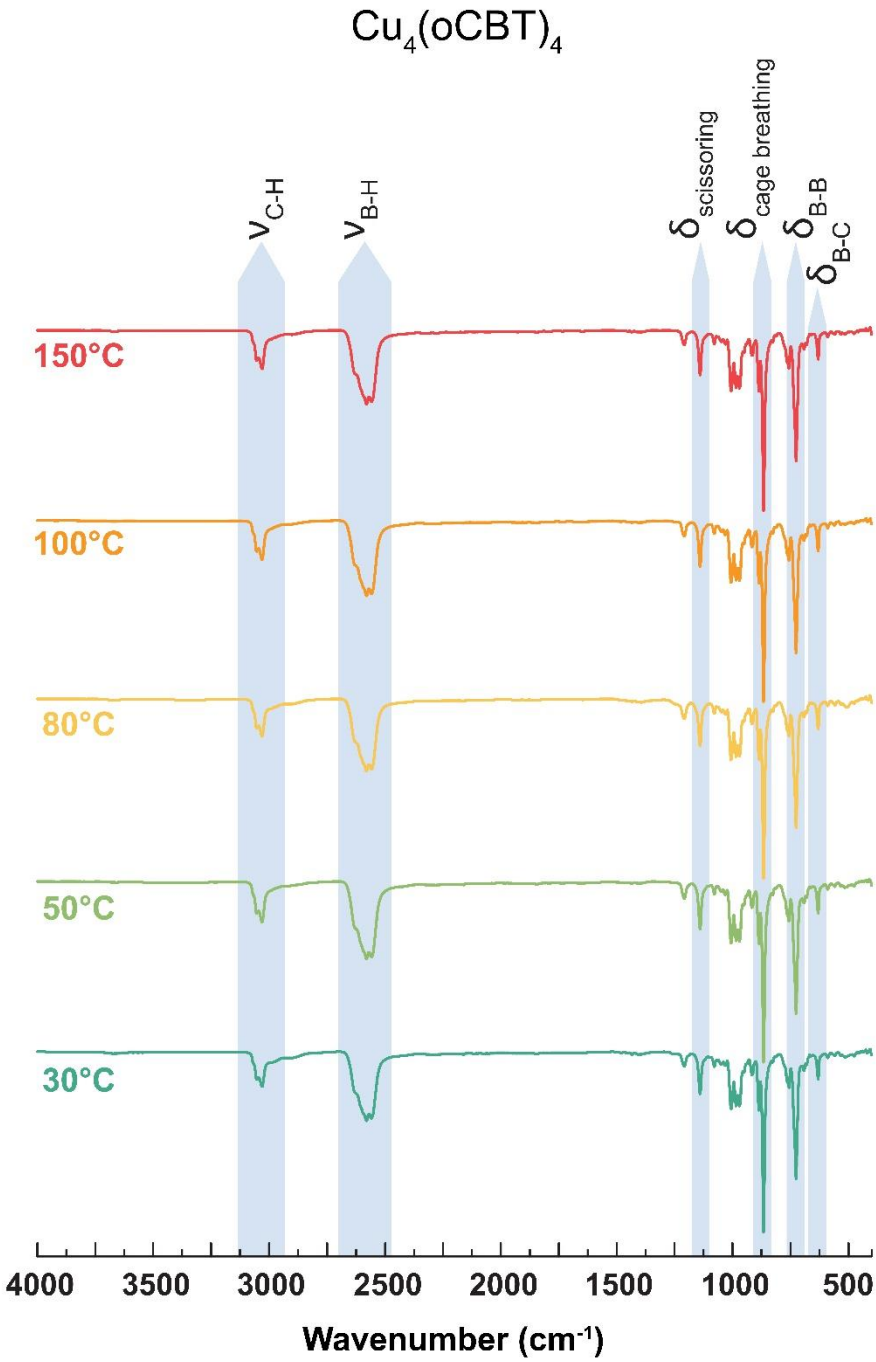

Figure S6. ATR- IR spectra of heat treated $Cu_4(oCBT)_4$ crystals showing the chemical stability of the samples up to 150°C.

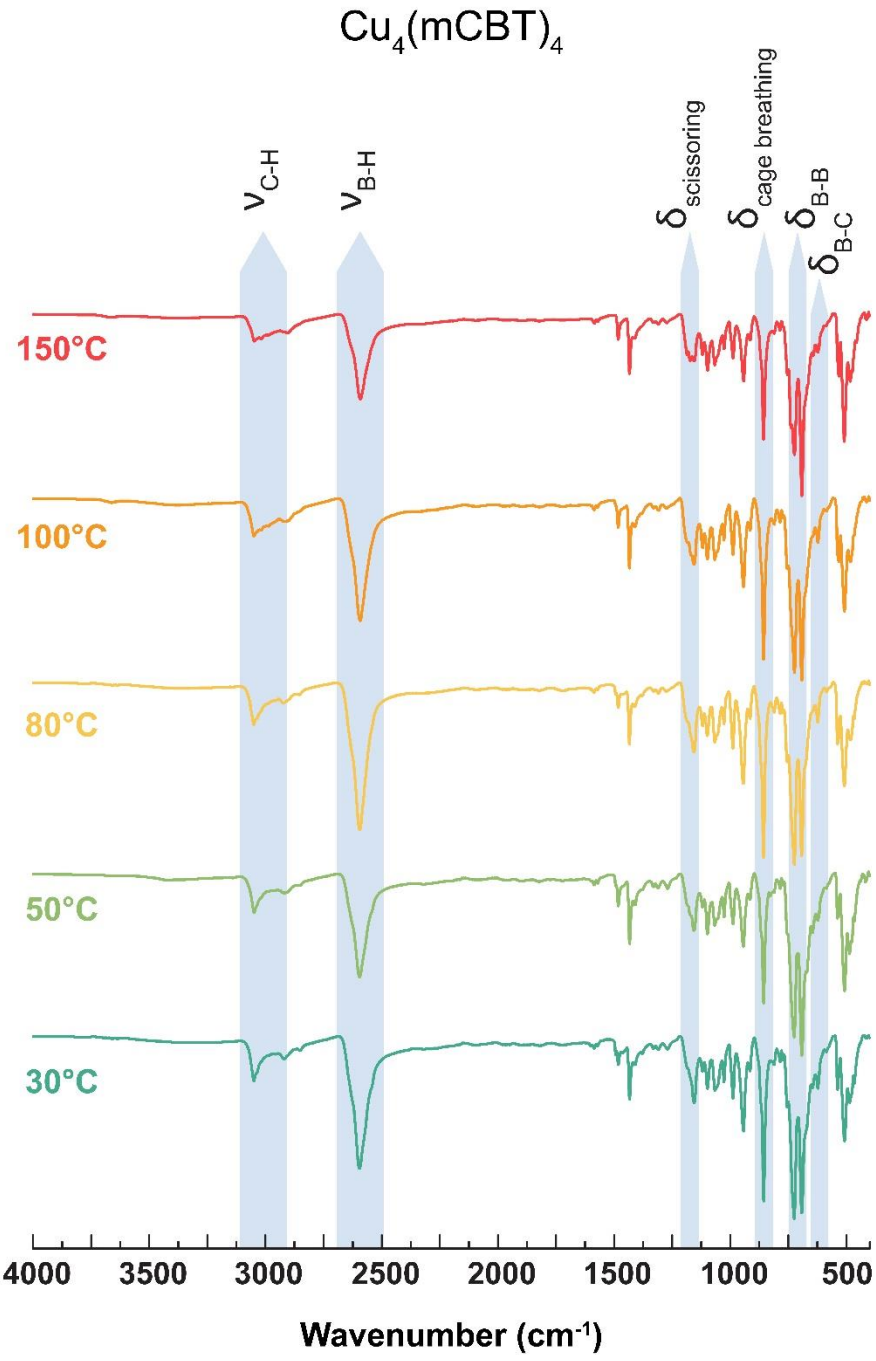

Figure S7. ATR- IR spectra of heat treated $Cu_4(mCBT)_4$ crystals showing the chemical stability of the samples up to 150°C

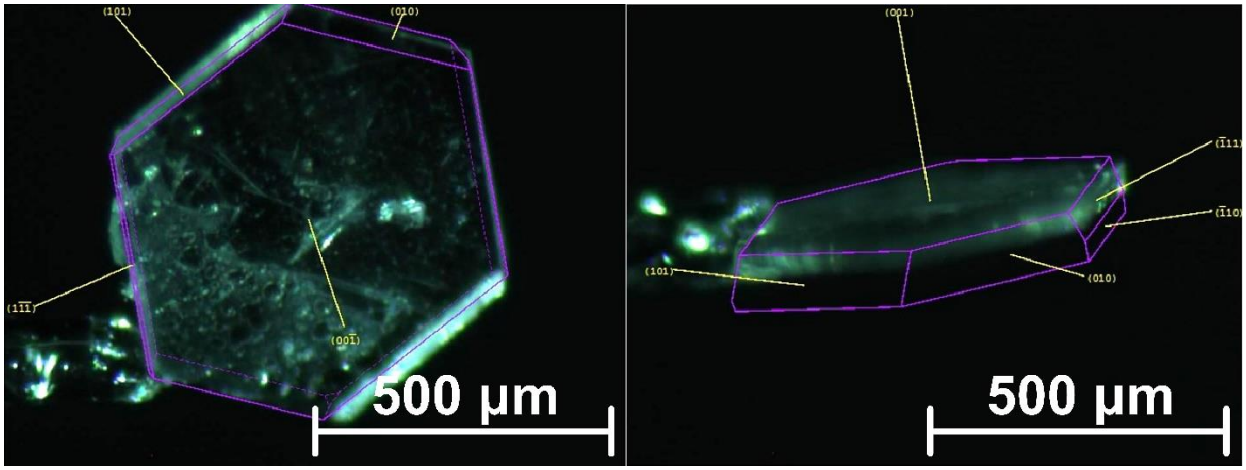

Figure S8. Face indexing of hexagonal $Cu_4(oCBT)_4$ single crystal from two different orientations.

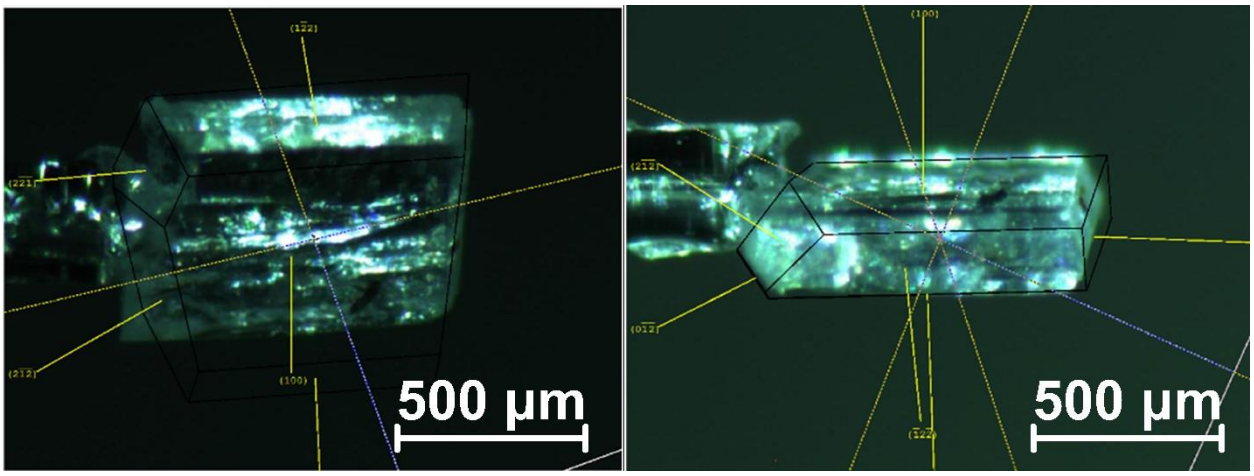

Figure S9. Face indexing of parallelepiped $Cu_4(mCBT)_4$ single crystal from two different orientations.

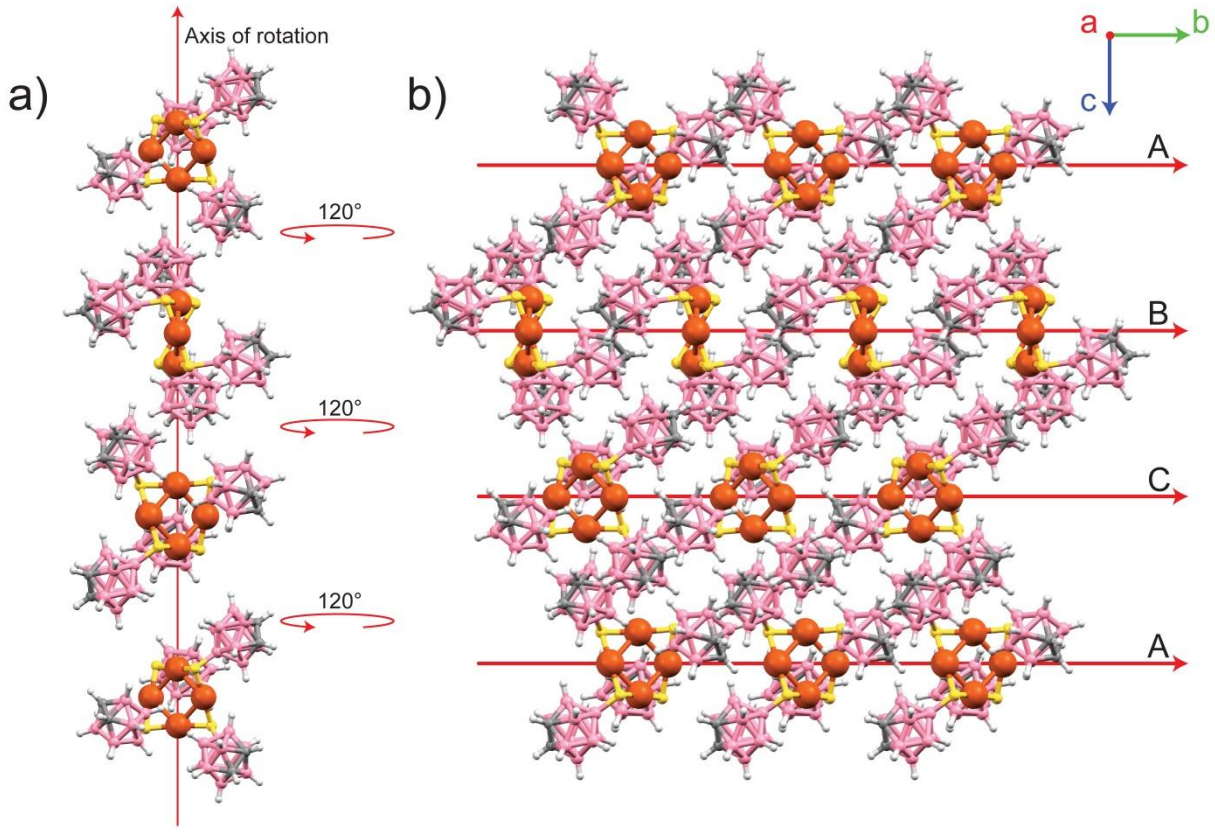

Figure S10. a) Orientation of each cluster with respect to the cluster in its upper layer showing 120° rotation along the axis of rotation. b) Extended packing structure of $Cu_4(oCBT)_4$ nanoclusters showing …ABCA… packing.

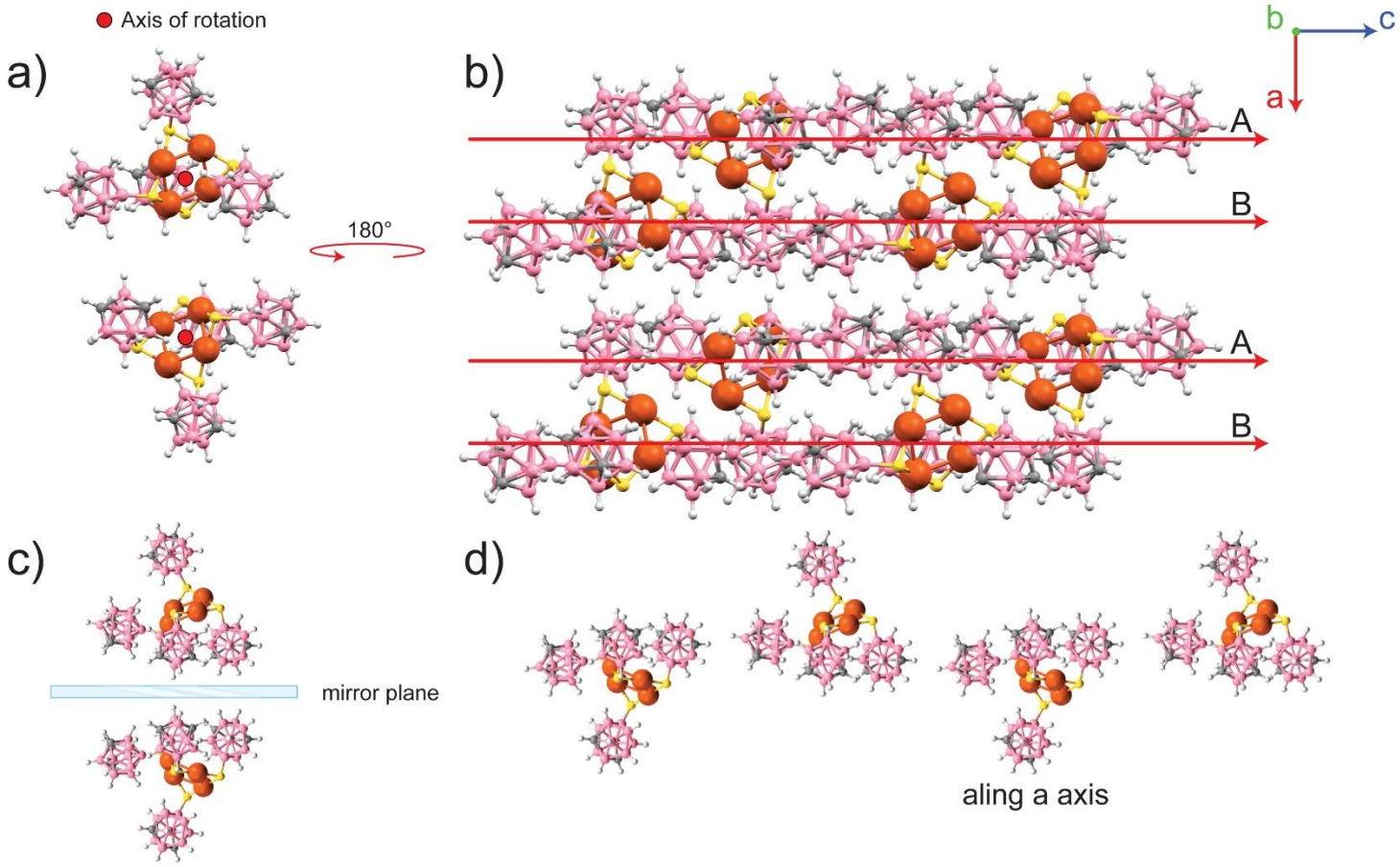

Figure S11. a) Orientation of each cluster with respect to the cluster in its upper layer showing 180° rotation along the axis of rotation. (Axis of rotation is perpendicular to the visible plane). b) Extended packing structure of $Cu_4(mCBT)_4$ nanoclusters showing …ABAB… packing. c) Shows the orientation of adjacent clusters as non-superimposable mirror images. An imaginary mirror plane is also shown. d) Adjacent clusters as observed along the *a* axis showing arrangement of clusters which are mirror images of each other.

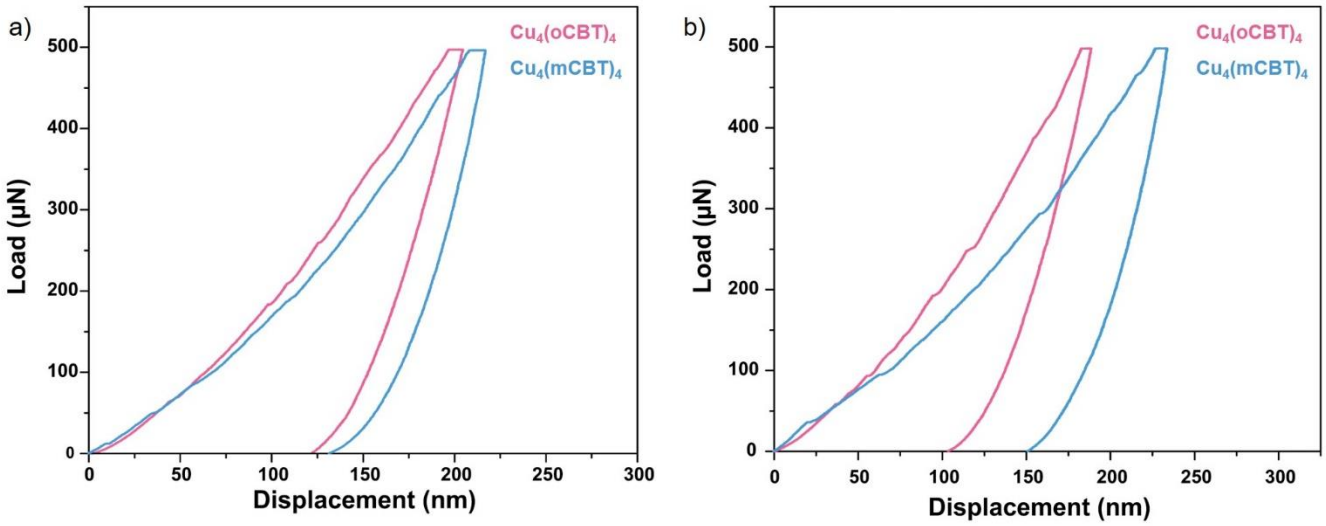

Figure S12. Load-controlled load-displacement curves of $Cu_4(oCBT)_4$ and $Cu_4(mCBT)_4$ crystals for a load of 500 μN with load functions a) 20_10_20 and b) 50_20_50.

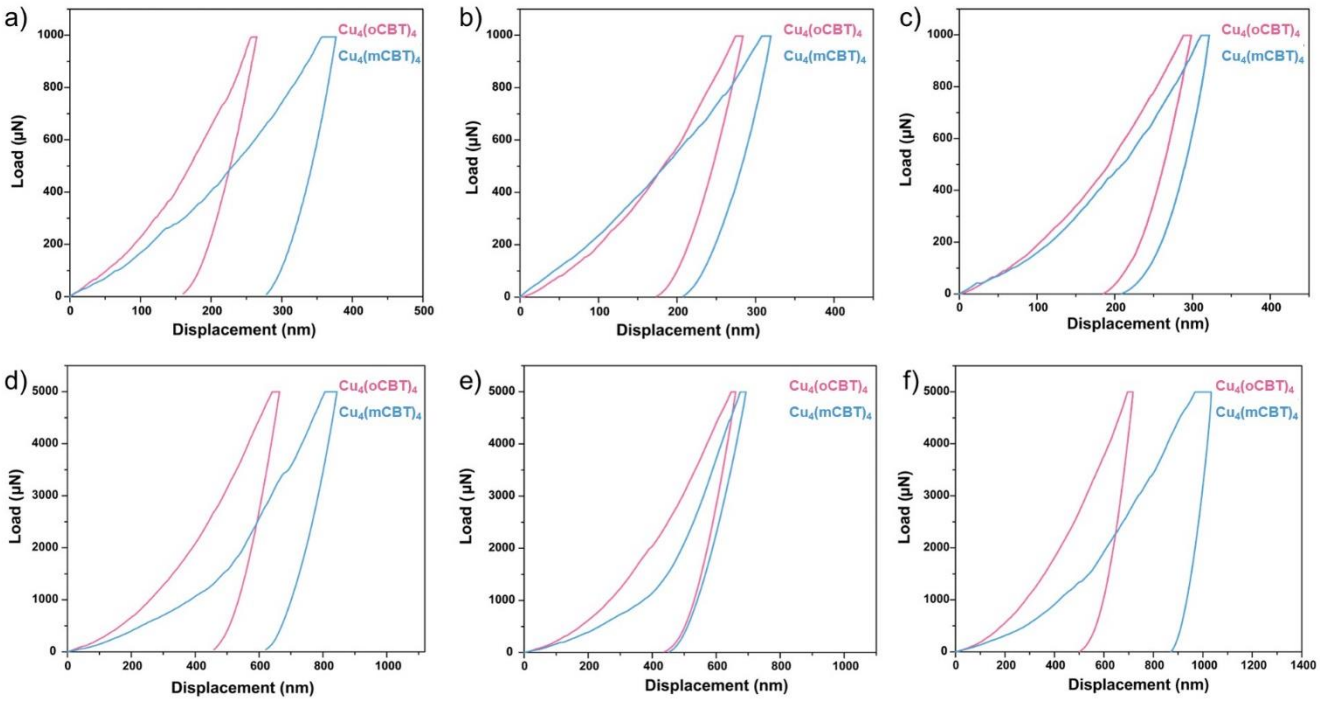

Figure S13. Load-controlled load-displacement curves of $Cu_4(oCBT)_4$ and $Cu_4(mCBT)_4$ crystals for a load of 1000 μN for a), b) and c) and a load of 5000 μN for d), e) and f) with load functions 5_10_5, 20_10_20 and 50_20_50, respectively.

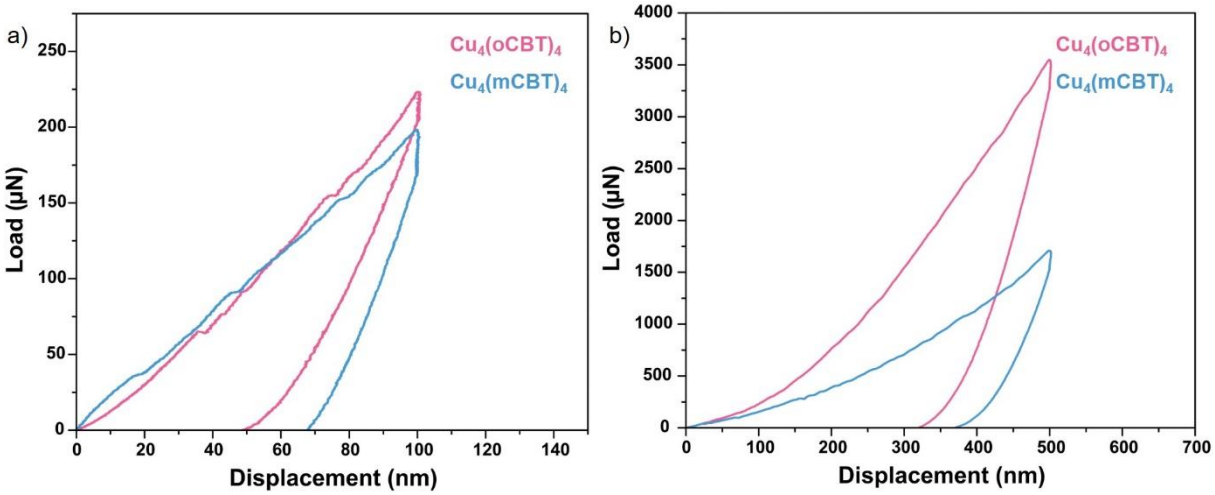

Figure S14. Displacement controlled load-displacement curves for $Cu_4(oCBT)_4$ and $Cu_4(mCBT)_4$ crystals with a fixed displacement of a) 100 nm and b) 500 nm.

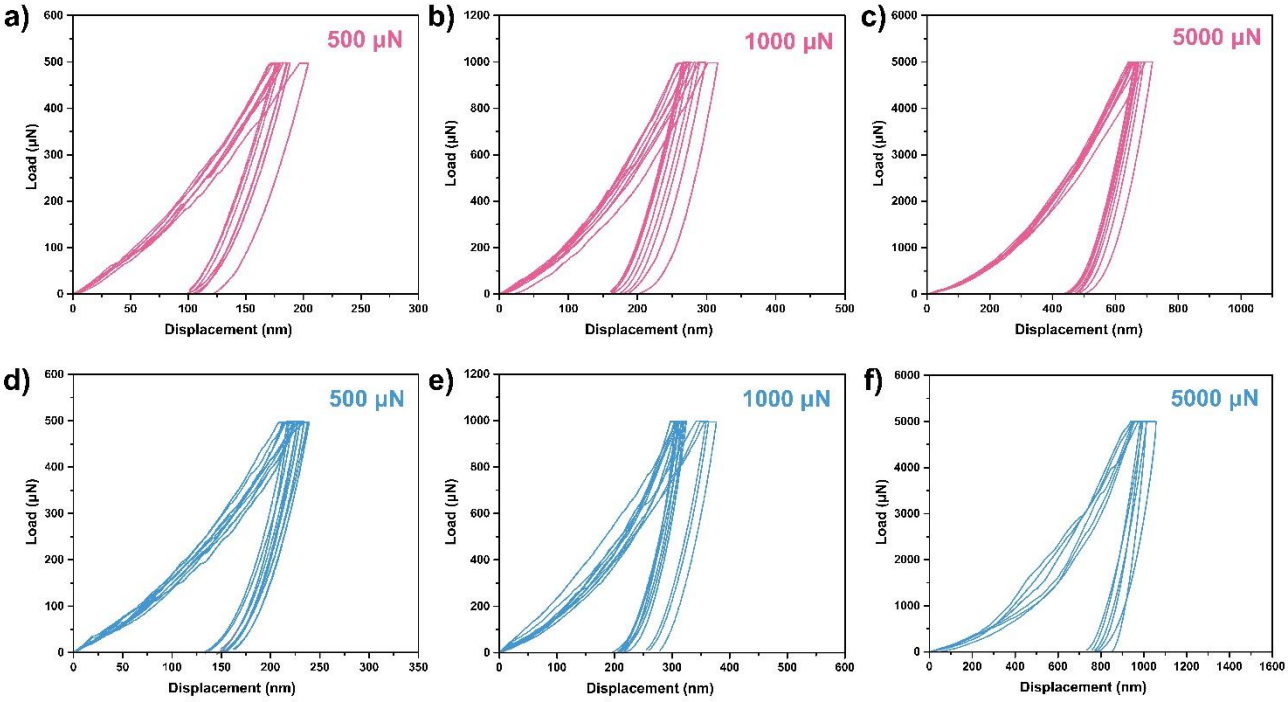

Figure S15. All the indentation measurements for $Cu_4(oCBT)_4$ (pink traces) and $Cu_4(mCBT)_4$ (blue traces) at varying loads; 500 μN (a and d), 1000 μN (b and e) and 5000 μN (c and f) plotted together to show the reproducibility for the measurements.

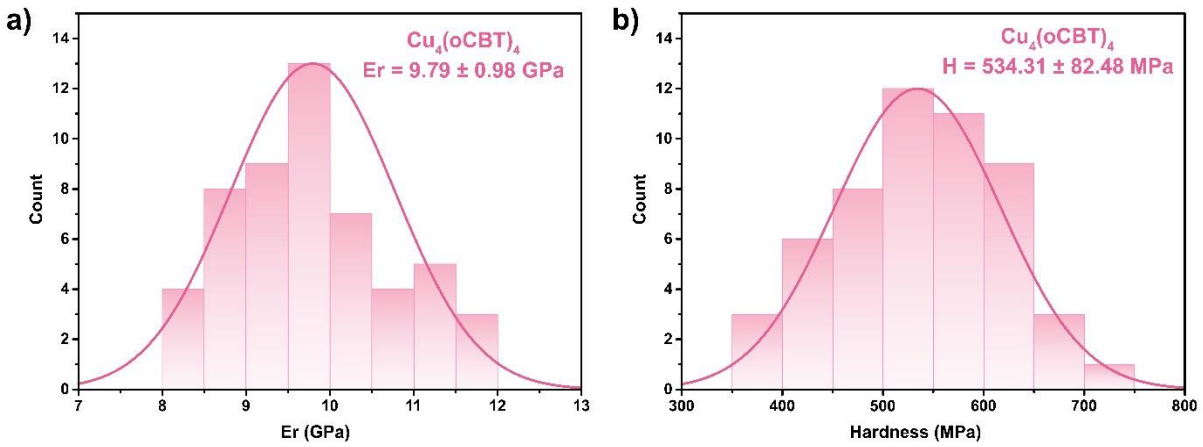

Figure S16. Statistical analysis of all the indentation data collected for $Cu_4(oCBT)_4$ nanocluster crystal. a) The distribution of the Young's modulus, Er, among the data sets collected. b) The distribution of Hardness, H, among the data sets collected.

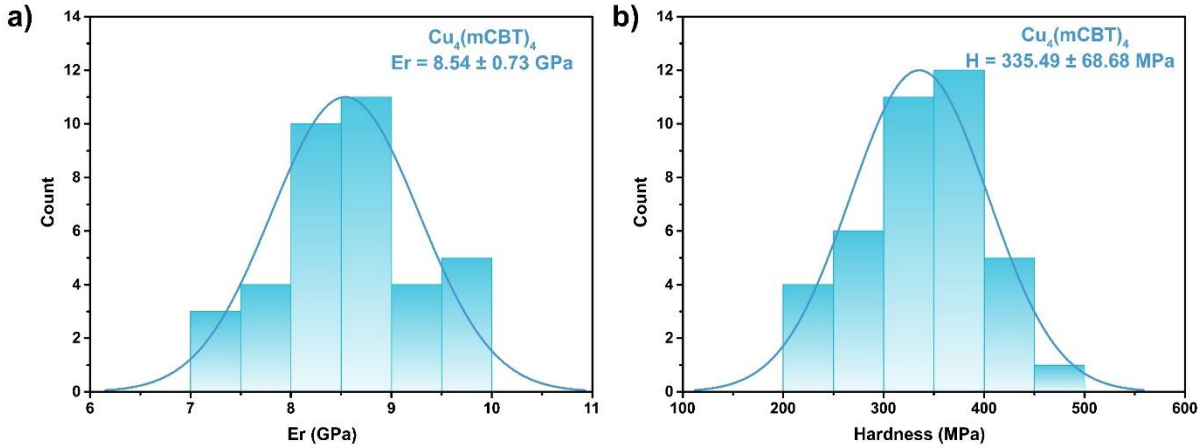

Figure S17. Statistical analysis of all the indentation data collected for $Cu_4(mCBT)_4$ nanocluster crystal. a) The distribution of the Young's modulus, Er, among the data sets collected. b) The distribution of Hardness, H, among the data sets collected.

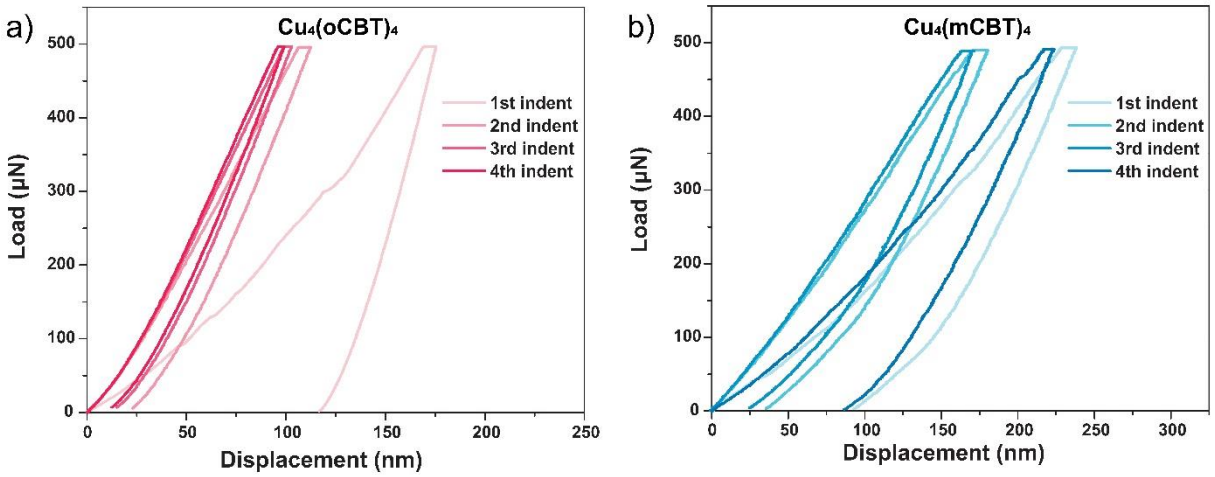

Figure S18. Load-displacement curves obtained by repeated indentations in the same place for a) Cu_4(o-CBT)$_4$ and b) Cu_4(m-CBT)$_4$, showing the indentation induced hardness in the crystals of the nanoclusters.

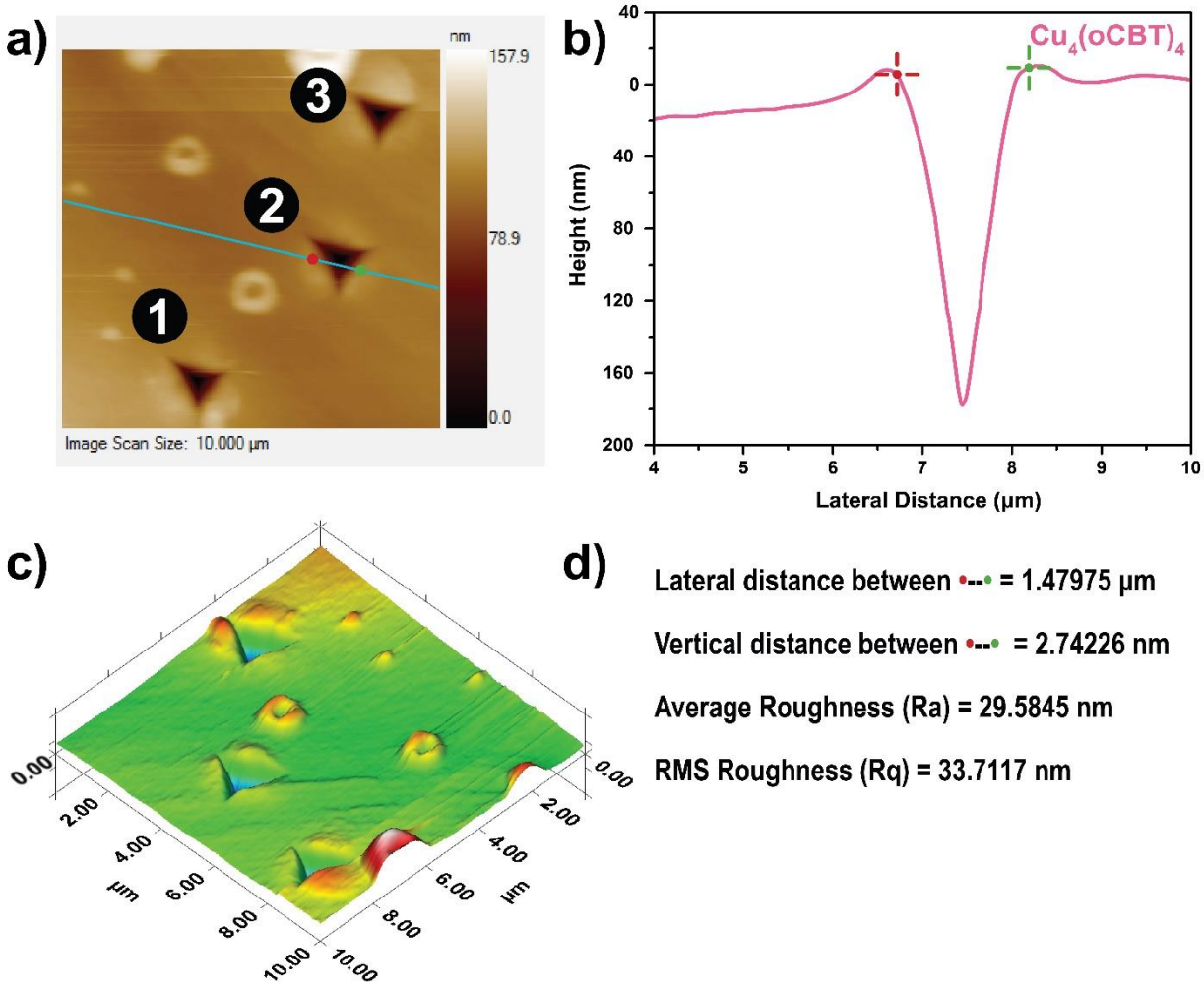

Figure S19. a) Scanning probe microscopy image of the surface of $Cu_4(oCBT)_4$ crystal after three indentations showing residual imprints on the surface with an applied load of 500 µN. b) Height profile of indentation **2** along the blue line. c) 3D projection of scanning probe microscopy image. d) Distance and roughness data between the red and green points shown in images a) and b).

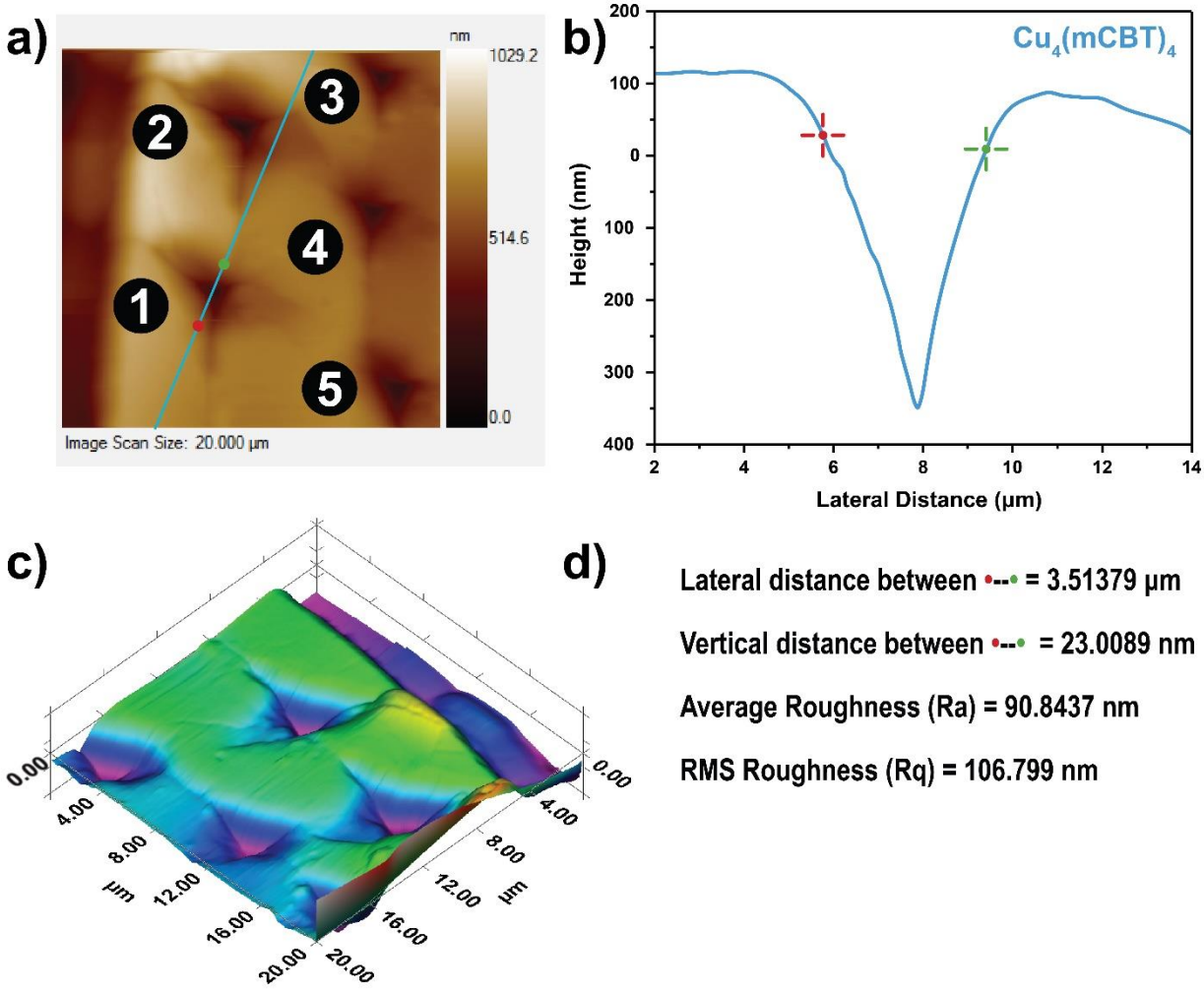

Figure S20. a) Scanning probe microscopy image of the surface of $Cu_4(mCBT)_4$ crystal after five indentations showing residual imprints on the surface with an applied load of 500 µN. b) Height profile of indentation **1** along the blue line. c) 3D projection of scanning probe microscopy image. d) Distance and roughness data between the red and green points shown in images a) and b).

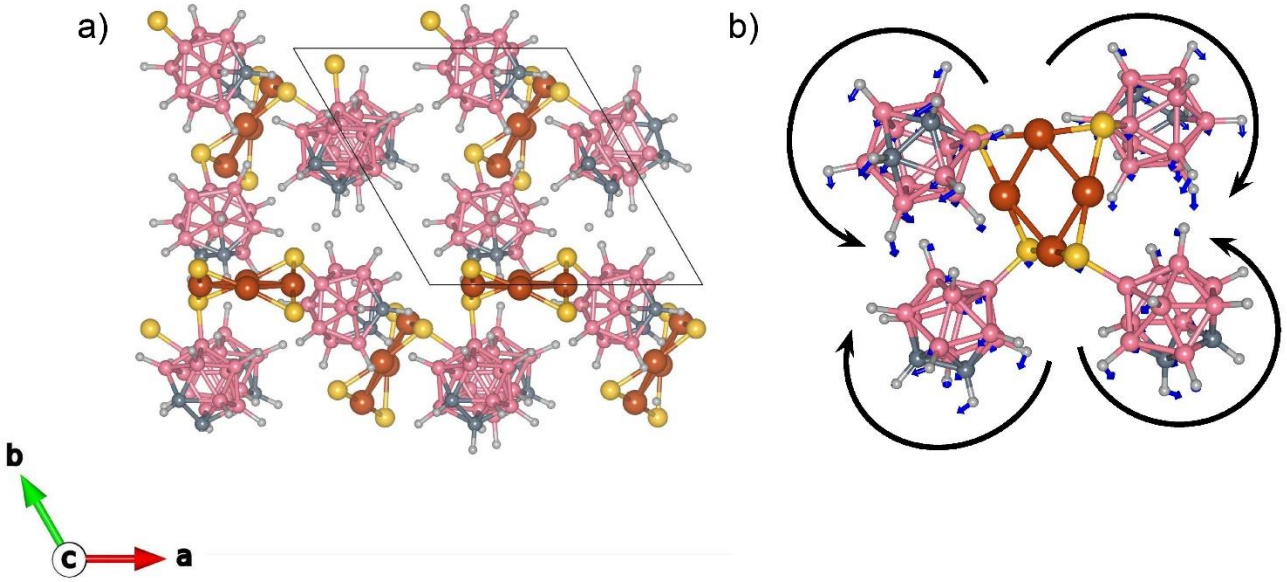

Figure S21. a) Arrangement of Cu_4 nanoclusters and ligands in the *ab* plane of $Cu_4(oCBT)_4$. The square planar Cu_4 clusters lie perpendicular to the plane, in the vacant space between oCBTs. b) Motion of various atoms in an isolated $Cu_4(oCBT)_4$ unit.

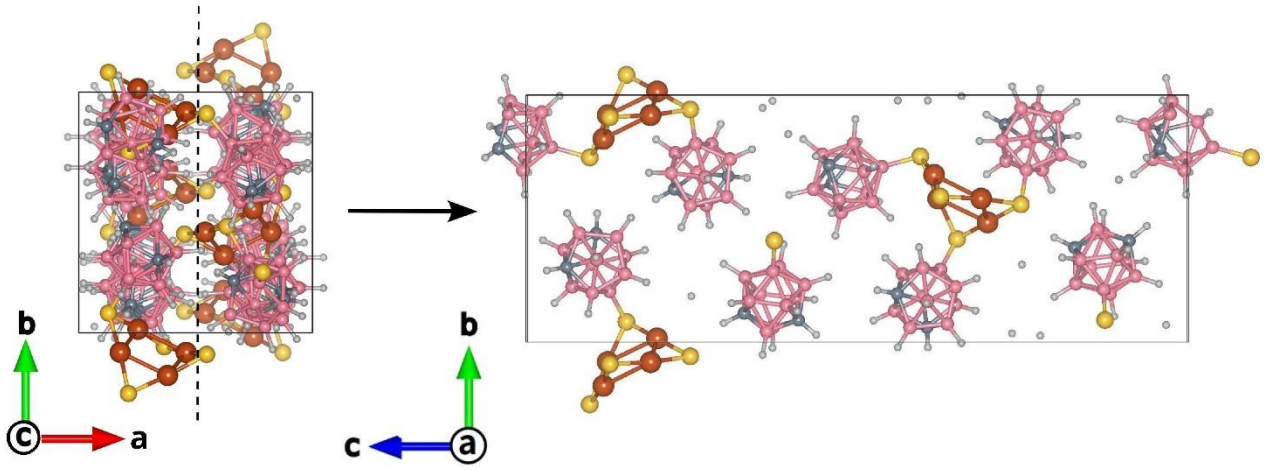

Figure S22. A transverse section of $Cu_4(mCBT)_4$ taken along the *a* axis reveals loosely packed CBT molecules attached to Cu_4 clusters.

Reference:

(1) Jana, A.; Jash, M.; Dar, W. A.; Roy, J.; Chakraborty, P.; Paramasivam, G.; Lebedkin, S.; Kirakci, K.; Manna, S.; Antharjanam, S.; Machacek, J.; Kucerakova, M.; Ghosh, S.; Lang, K.; Kappes, M. M.; Base, T.; Pradeep, T. Carborane-Thiol Protected Copper Nanoclusters: Stimuli-Responsive Materials with Tunable Phosphorescence. *Chem. Sci.* **2023**, *14* (6), 1613–1626. https://doi.org/10.1039/D2SC06578A.